

Mapping gauged Q -balls

Julian Heeck^{*}

Department of Physics, University of Virginia, Charlottesville, Virginia 22904-4714, USA

Arvind Rajaraman,[†] Rebecca Riley[‡], and Christopher B. Verhaar[§]

Department of Physics and Astronomy, University of California, Irvine, California 92697-4575, USA



(Received 13 April 2021; accepted 6 May 2021; published 4 June 2021)

Scalar field theories with particular $U(1)$ -symmetric potentials contain nontopological soliton solutions called Q -balls. Promoting the $U(1)$ to a gauge symmetry leads to the more complicated situation of gauged Q -balls. The soliton solutions to the resulting set of nonlinear differential equations have markedly different properties, such as a maximal possible size and charge. Despite these differences, we discover a relation that allows one to extract the properties of gauged Q -balls (such as the radius, charge, and energy) from the more easily obtained properties of global Q -balls. These results provide a new guide to understanding gauged Q -balls as well as providing simple and accurate analytical characterization of the Q -ball properties.

DOI: [10.1103/PhysRevD.103.116004](https://doi.org/10.1103/PhysRevD.103.116004)

I. INTRODUCTION

Q -balls are stable nontopological solitons that can arise in theories involving complex scalars ϕ [1] (for a review, see Ref. [2]). In the case of global Q -balls, ϕ carries a conserved global charge and the solitons are stabilized by a scalar potential that provides an attractive force [3]. Global Q -balls have been proposed as dark matter [4,5] due to their potential occurrence in supersymmetric models and provide in particular a simple realization of macroscopic dark matter [6,7].

The analytic construction of Q -balls requires solving a nonlinear differential equation. In certain potentials, the equation can be solved exactly [8–11]. For many other cases, numerical solutions can be efficiently obtained via computer programs such as AnyBubble [12]. Recently, it was shown that almost all aspects of global Q -balls can be understood essentially analytically, even for potentials which are not exactly solvable [13]. Extremely accurate analytical expressions were obtained for global Q -ball properties such as radius, charge, and energy in some nonsolvable scenarios which essentially obviate the need for numerical studies [13]. It appears that for all intents and purposes single-field global Q -balls are a solved problem.

The system's complexity increases if ϕ is charged under a local symmetry, which leads to *gauged* Q -balls [14–16]. Given the prevalence of gauge bosons in the Standard Model and its extensions, understanding gauged Q -balls is important phenomenologically. However, they are considerably more difficult to describe, both analytically and numerically. On the analytic side, no exactly solvable examples are known to us. Numerical studies are made difficult by the gauge field, which appears in the scalar potential as a field whose kinetic term has the opposite sign. This makes numerical studies (using, e.g., the ever-popular shooting method) far more tedious to implement.

In this paper, we extend the methods of Ref. [13] to gauged Q -balls. In so doing, we reveal a close connection between global Q -balls and gauged Q -balls. This enables us to use our understanding of global Q -balls to analytically calculate the properties of these gauged Q -balls—such as radius, charge, and energy. Furthermore, we find simple expressions for the scalar and gauge field profiles that can be used to solve the differential equations efficiently using finite-element methods. This work paves the way for detailed phenomenological studies of these objects.

In the next section, we review global Q -balls and establish our notation. Section III introduces gauged Q -balls and analytical approximations for the scalar and gauge field profiles. In Sec. IV, we present a method for solving the Q -ball differential equations using finite-element methods rather than the shooting method. The novel mapping between global and gauged solutions is given in Sec. V. The accuracy of our analytical predictions for the Q -ball profiles and observables, such as energy, mass, and radius, is established in Sec. VI. We also derive quantities of interest such as the parametric regions of

^{*}heck@virginia.edu

[†]arajaram@uci.edu

[‡]rebecca.riley@uci.edu

[§]cverhaar@uci.edu

Published by the American Physical Society under the terms of the Creative Commons Attribution 4.0 International license. Further distribution of this work must maintain attribution to the author(s) and the published article's title, journal citation, and DOI. Funded by SCOAP³.

Q-ball stability before concluding in Sec. VII. A derivation of the Q-ball energy and alternative derivation of the mapping formula is given in Appendixes A and B, respectively.

II. REVIEW OF GLOBAL Q-BALLS

The Lagrangian density for a complex scalar ϕ ,

$$\mathcal{L} = |\partial_\mu \phi|^2 - U(|\phi|), \quad (1)$$

enjoys an explicit global $U(1)$ symmetry $\phi \rightarrow e^{i\alpha}\phi$. The conserved charge Q under this symmetry is ϕ number, normalized so that $Q(\phi) = 1$. To preserve the $U(1)$ symmetry, we require $\langle \phi \rangle = 0$ in the vacuum. We choose the potential energy to be zero in the vacuum by setting $U(0) = 0$ and enforce that the vacuum is a stable minimum of the potential by

$$\left. \frac{dU}{d|\phi|} \right|_{\phi=0} = 0, \quad \left. \frac{d^2U}{d\phi d\phi^*} \right|_{\phi=0} = m_\phi^2, \quad (2)$$

where m_ϕ is the mass of the complex scalar. In this scenario, Coleman [1] showed that nontopological solitons, Q-balls, exist when the function $U(|\phi|)/|\phi|^2$ has a minimum at $0 < \phi_0 < \infty$ such that

$$0 \leq \sqrt{\frac{2U(\phi_0)}{\phi_0^2}} \equiv \omega_0 < m_\phi. \quad (3)$$

Spherical Q-ball solutions have the form

$$\phi(t, \vec{x}) = \frac{\phi_0}{\sqrt{2}} f(r) e^{i\omega_G t} \quad (4)$$

for a constant $\omega_0 < \omega_G < m_\phi$. We choose ω_G to be positive, which results in a positive charge Q of the Q-ball. It is convenient to define the dimensionless quantities

$$\begin{aligned} \rho &\equiv r \sqrt{m_\phi^2 - \omega_0^2}, & \Omega_G &\equiv \frac{\omega_G}{\sqrt{m_\phi^2 - \omega_0^2}}, \\ \Omega_0 &\equiv \frac{\omega_0}{\sqrt{m_\phi^2 - \omega_0^2}}, & \Phi_0 &\equiv \frac{\phi_0}{\sqrt{m_\phi^2 - \omega_0^2}}. \end{aligned} \quad (5)$$

We can then write the Lagrangian as

$$\begin{aligned} L = 4\pi\Phi_0^2 \sqrt{m_\phi^2 - \omega_0^2} \int d\rho \rho^2 &\left[-\frac{1}{2} f'^2 + \frac{1}{2} f^2 \Omega_G^2 \right. \\ &\left. - \frac{U(f)}{\Phi_0^2 (m_\phi^2 - \omega_0^2)^2} \right], \end{aligned} \quad (6)$$

where a prime denotes a derivative with respect to ρ . The equation of motion for f is

$$f'' + \frac{2}{\rho} f' = \frac{1}{\Phi_0^2 (m_\phi^2 - \omega_0^2)^2} \frac{dU}{df} - \Omega_G^2 f. \quad (7)$$

Q-ball solutions for f satisfy this nonlinear differential equation along with the boundary conditions $f'(\rho \rightarrow 0) = 0 = f(\rho \rightarrow \infty)$.

As an explicit example, we consider the most generic $U(1)$ -symmetric sextic potential studied in Ref. [13]. This can be parametrized as

$$U(f) = \phi_0^2 \left(\frac{m_\phi^2 - \omega_0^2}{2} f^2 (1 - f^2)^2 + \frac{\omega_0^2}{2} f^2 \right). \quad (8)$$

The differential equation of Eq. (7) then takes the form

$$f'' + \frac{2}{\rho} f' = f(1 - \kappa_G^2 - 4f^2 + 3f^4), \quad (9)$$

where $\kappa_G^2 \equiv \Omega_G^2 - \Omega_0^2$. The solutions depend on the single parameter $\kappa_G \in (0, 1)$, which also determines the (dimensionless) Q-ball radius R^* .¹

For small κ_G , the Q-balls are large and the relation $R^*(\kappa_G)$ can be calculated analytically at leading order to be $R^*(\kappa_G) = 1/\kappa_G^2$ [13]. For these large Q-balls, the exact Q-ball profile is close to a step function $f(\rho) \simeq 1 - \Theta(\rho - R^*)$; this is the so-called *thin-wall* limit [1]. As shown in Ref. [13], an even better profile for these thin-wall Q-balls around $\rho \sim R^* \gg 1$ is

$$f_T(\rho) = \frac{1}{\sqrt{1 + 2e^{2(\rho - R^*)}}}. \quad (10)$$

This is called the transition profile, since it describes the rapid transition from the nearly constant $f \simeq 1$ inside the Q-ball to $f \simeq 0$ outside the Q-ball. The transition profile is actually a very good approximation to the full profile for all ρ and even works reasonably well for smaller Q-balls [13].

We also present here a new relation for $R^*(\kappa_G)$,

$$R^*(\kappa_G) = \frac{1}{\kappa_G^2} - \frac{1}{4\kappa_G} + \frac{3}{2} - 2\kappa_G + \frac{1}{3\sqrt{1 - \kappa_G^2}}, \quad (11)$$

which provides an approximation to the numerical result (shown in Fig. 1), that is accurate to better than 2% in the region $\kappa_G < 0.84$ (or $R^* \gtrsim 1.5$) that leads to stable Q-balls (i.e., Q-balls with $E < m_\phi Q$). This relation can be used to produce extremely accurate expressions of the global

¹The definition of R^* is somewhat ambiguous as f transitions smoothly from its value at the center of the Q-ball to its value outside, but a useful definition is $f''(\rho = R^*) = 0$.

Q-ball's energy and charge as a function of radius using the expressions in Ref. [13].

III. GAUGED Q-BALLS

Gauged Q-balls result from promoting the global $U(1)$ symmetry to a local symmetry. The Lagrangian density is

$$\mathcal{L} = |D_\mu \phi|^2 - U(|\phi|) - \frac{1}{4} F_{\mu\nu} F^{\mu\nu}, \quad (12)$$

where $D_\mu = \partial_\mu - ieA_\mu$ is the gauge covariant derivative and $F_{\mu\nu} = \partial_\mu A_\nu - \partial_\nu A_\mu$ is the field-strength tensor. The parameter e is the gauge coupling normalized so that ϕ has charge one. After making the static charge ansatz [14],

$$\phi(t, \vec{x}) = \frac{\phi_0}{\sqrt{2}} f(r) e^{i\omega t}, \quad A_0(t, \vec{x}) = A_0(r), \quad A_i(t, \vec{x}) = 0, \quad (13)$$

and defining dimensionless quantities

$$\Omega \equiv \frac{\omega}{\sqrt{m_\phi^2 - \omega_0^2}}, \quad A(\rho) \equiv \frac{A_0(\rho)}{\phi_0}, \quad \alpha \equiv e\Phi_0, \quad \kappa^2 \equiv \Omega^2 - \Omega_0^2, \quad (14)$$

we rewrite the Lagrangian as

$$L = 4\pi\Phi_0^2 \sqrt{m_\phi^2 - \omega_0^2} \int d\rho \rho^2 \left\{ -\frac{1}{2} f'^2 + \frac{1}{2} A'^2 + \frac{1}{2} f^2 (\Omega - \alpha A)^2 - \frac{U(f)}{\Phi_0^2 (m_\phi^2 - \omega_0^2)^2} \right\}. \quad (15)$$

This has the form of two scalar fields under the influence of the potential

$$V(f, A) = \frac{1}{2} f^2 (\Omega - \alpha A)^2 - \frac{U(f)}{\Phi_0^2 (m_\phi^2 - \omega_0^2)^2}. \quad (16)$$

However, it is important to notice that in this analogy the A field's kinetic term has the wrong sign. The two equations of motion

$$f'' + \frac{2}{\rho} f' = -\frac{\partial V}{\partial f} = \frac{1}{\Phi_0^2 (m_\phi^2 - \omega_0^2)^2} \frac{dU}{df} - (\Omega - \alpha A)^2 f, \quad (17)$$

$$A'' + \frac{2}{\rho} A' = +\frac{\partial V}{\partial A} = \alpha f^2 (\alpha A - \Omega) \quad (18)$$

are to be solved subject to the boundary conditions

$$\lim_{\rho \rightarrow 0} f' = \lim_{\rho \rightarrow \infty} f = \lim_{\rho \rightarrow 0} A' = \lim_{\rho \rightarrow \infty} A = 0. \quad (19)$$

In the analogy of two fields moving in the potential V , ρ becomes a time coordinate and the terms with an explicit $1/\rho$ can be interpreted as time-dependent friction terms. As shown below, this analogy greatly aids our understanding of the Q-ball solutions.

The scalar frequency ω is restricted to the region $\omega_0 < \omega \leq m_\phi$; this is similar to the global Q-ball case, except that it is possible to have gauged Q-balls with $\omega = m_\phi$ (or $\kappa = 1$) [15], where no global Q-balls exist. In Sec. VI, we show that a stronger lower bound on ω exists.

The conserved charge Q is defined in the usual way as the integral over the time component of the scalar current [14]

$$Q = 4\pi\Phi_0^2 \int d\rho \rho^2 f^2 (\Omega - \alpha A) \quad (20)$$

$$= -\frac{4\pi\Phi_0^2}{\alpha} \lim_{\rho \rightarrow \infty} \rho^2 A', \quad (21)$$

where the second line uses Eq. (18) and integration by parts. This implies that for large ρ ,

$$A = \frac{\alpha Q}{4\pi\Phi_0^2 \rho}, \quad (22)$$

up to corrections that fall off faster than $1/\rho$ [14]. The gauged Q-ball energy E is obtained from the Hamiltonian,

$$E/\sqrt{m_\phi^2 - \omega_0^2} = 4\pi\Phi_0^2 \int d\rho \rho^2 \left\{ \frac{1}{2} f'^2 + \frac{1}{2} A'^2 + \frac{1}{2} f^2 (\Omega - \alpha A)^2 + \frac{U(f)}{\Phi_0^2 (m_\phi^2 - \omega_0^2)^2} \right\} \quad (23)$$

$$= \Omega Q + \frac{4\pi\Phi_0^2}{3} \int d\rho \rho^2 (f'^2 - A'^2). \quad (24)$$

The second expression corrects a typo in Ref. [14] and is derived in Appendix A. The energy and charge also satisfy the nontrivial differential equation [17]

$$\frac{dE}{d\omega} = \omega \frac{dQ}{d\omega}. \quad (25)$$

This is a powerful relation among the Q-ball observables and, in particular, allows ω to be interpreted as the chemical potential.

For concreteness, we restrict most of our discussion to the sextic scalar potential of Eq. (8), although we expect our results to be qualitatively applicable to a far larger class of potentials. Just like in the global case we only study

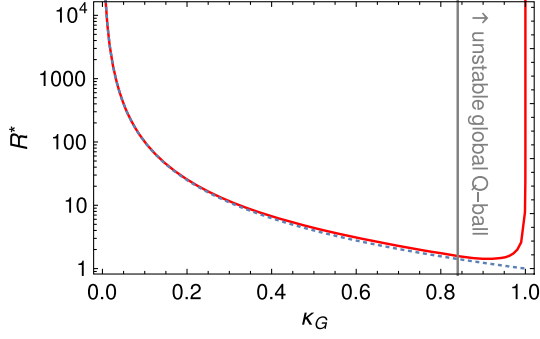


FIG. 1. The global Q-ball radius R^* vs $\kappa_G = \sqrt{\Omega_G^2 - \Omega_0^2}$ for the sextic potential [13] in red. The blue dotted line shows the approximation $\kappa_G^2 = 1/R^*$. The region $\kappa_G \gtrsim 0.84$ leads to unstable global Q-balls due to $E > m_\phi Q$ [13].

ground-state Q-balls, which have no nodes; excited gauged Q-balls in the same potential have been discussed in Ref. [18].

IV. NUMERICAL METHODS

While the shooting method is quite successful for global Q-balls [1], the addition of the gauge field makes finding a solution using this method tedious, especially for large Q-balls. We avoid this by changing coordinates and solving the boundary value problem directly. A similar approach was employed in Ref. [19].

In order to enforce the boundary conditions at $\rho = \infty$, we switch to a compactified coordinate y ,

$$y = \frac{\rho}{1 + \rho/a}, \quad (26)$$

where a is a positive constant. The value of a makes no real difference in obtaining numerical solutions. However, choosing a much larger than the Q-ball radius ensures that the most drastic compactification effects occur outside the Q-ball. Clearly, y takes values $y \in [0, a]$ and so we can require the conditions $f(a) = 0$ and $A(a) = 0$. The derivatives become

$$\frac{d}{d\rho} = \frac{dy}{d\rho} \frac{d}{dy} = \left(1 - \frac{y}{a}\right)^2 \frac{d}{dy}, \quad (27)$$

so the boundary conditions at $y = 0$ are $f'(0) = 0$ and $A'(0) = 0$ where primes denote a derivative with respect to y . The set of equations

$$\left(1 - \frac{y}{a}\right)^4 \left(f'' + \frac{2}{y}f'\right) + f(\kappa^2 + \alpha A(\alpha A - 2\Omega) - 1 + 4f^2 - 3f^4) = 0, \quad (28)$$

$$\left(1 - \frac{y}{a}\right)^4 \left(A'' + \frac{2}{y}A'\right) - \alpha f^2(\alpha A - \Omega) = 0 \quad (29)$$

can then be solved by finite-element methods, using *Mathematica's* [20] routines, for instance, and quickly converges to the exact solution if the initial guess is reasonably accurate. In the next section, we present a method for finding analytical test functions for f and A that are close to the exact solutions. These can be successfully used as initial seed functions for this method.

V. MAPPING GLOBAL Q-BALLS TO GAUGED Q-BALLS

Much of the Q-ball profile can be understood by comparing it to the motion of a particle moving in the potential of Eq. (16),

$$V(f, A) = \frac{1}{2}f^2[\kappa^2 + \alpha A(\alpha A - 2\Omega) - (1 - f^2)^2]. \quad (30)$$

For constant A , the potential in $f \geq 0$ has three extrema, one at $f = 0$ and the other two at

$$f_\pm^2 = \frac{1}{3} \left(2 \pm \sqrt{1 + 3\kappa^2 - 3\alpha A(2\Omega - \alpha A)} \right), \quad (31)$$

f_+ being a maximum and f_- a minimum.

For *global* Q-balls, the second term in $V(f, 0)$ vanishes; the scalar field starts close to the top of the potential at $f \approx f_+(A = 0)$. Eventually, the scalar rolls off and transitions to the second maximum at $f = 0$. Figure 2 gives an example global profile (blue curve of the left panel) along with the potential that determines its dynamics (right panel). Black points on the potential mark values of integer ρ and illustrate that the field is nearly constant until $\rho \approx 20$, after which the field rolls quickly. The initial location of the field profile on the potential was found in Ref. [13] by matching the energy gap between the initial and final maxima to the loss of energy due to the frictionlike term in the equation of motion.

Similar arguments apply to gauged Q-balls. The primary difference between the global and gauged cases is that the evolving gauge field A causes the effective potential for the scalar to change with ρ ; see the left panel of Fig. 3. The gauge field evolution changes the location and height of the second maximum at f_+ , and the scalar continues to follow this maximum until a certain point when it transitions quickly to the other maximum at $f = 0$. Of course, this can only occur when f_+ exists, so the requirement that Eq. (31) is real implies

$$\frac{1}{3} + \kappa^2 \geq \alpha A(2\Omega - \alpha A). \quad (32)$$

Notice that this condition is trivially satisfied in the global case, i.e., for $\alpha \rightarrow 0$, but in the gauged case restricts αA to two possible regions,

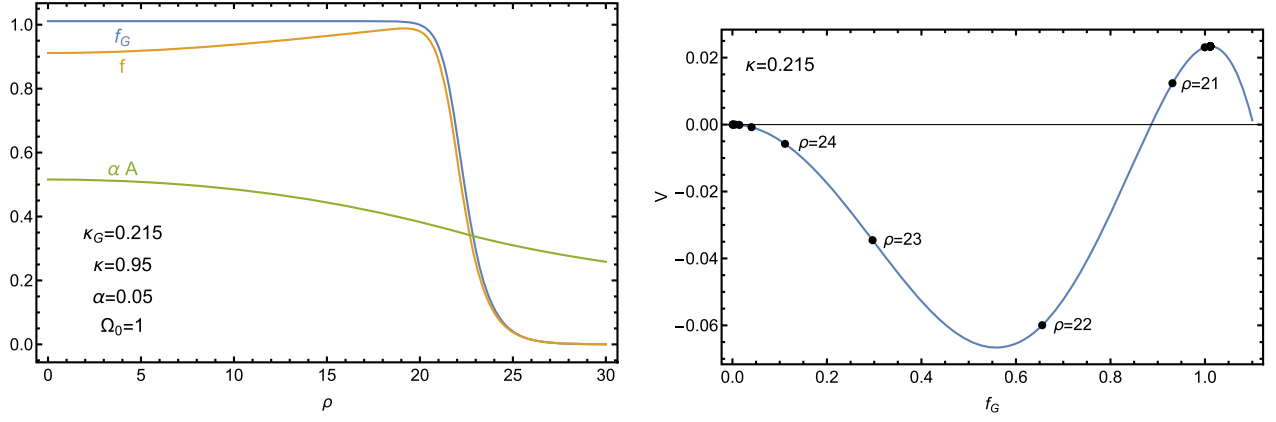


FIG. 2. Left: profiles for global f_G and gauged f , αA Q -balls corresponding to $R^* \approx 22$. Right: effective potential for the global Q -ball. Black points indicate the value of f_G for integer values of $\rho \in [0, 30]$.

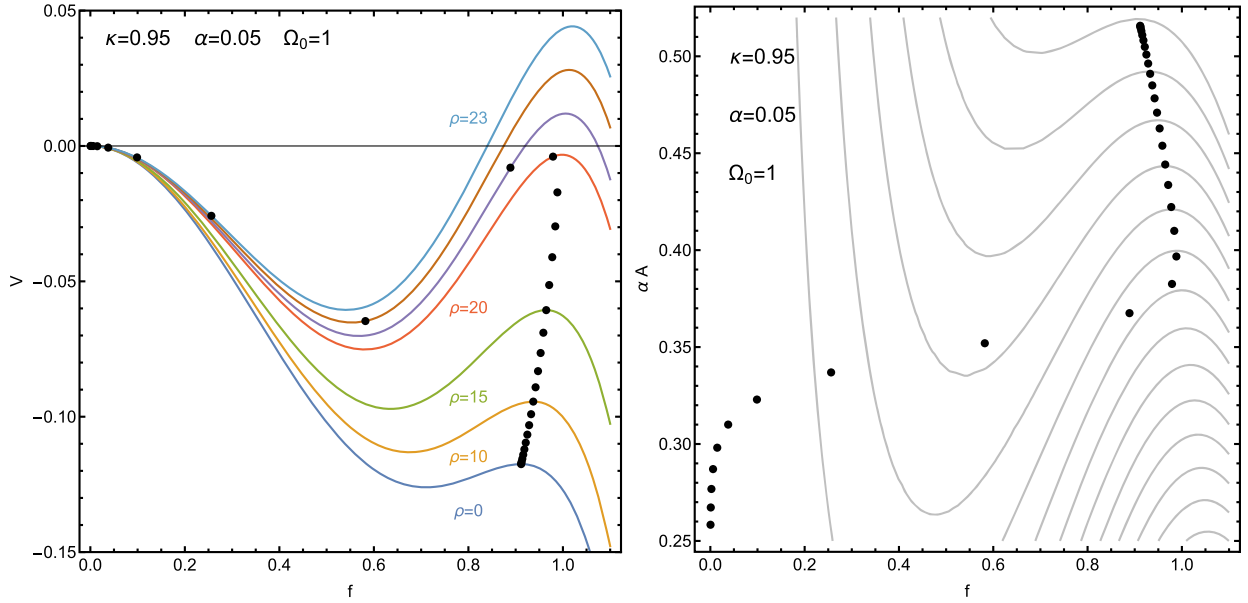


FIG. 3. Black points indicate the values of the gauged Q -ball profiles for integer values of $\rho \in [0, 30]$. Left: effective potentials for f given for specific values of $A(\rho)$. Right: contour plot of the potential V as a function of f and αA .

$$\alpha A \leq \Omega - \sqrt{\Omega_0^2 - \frac{1}{3}} \quad \text{or} \quad \alpha A \geq \Omega + \sqrt{\Omega_0^2 - \frac{1}{3}}. \quad (33)$$

As shown below, the second inequality in Eq. (33) is not compatible with Q -ball solutions, leaving us with an *upper* bound on αA when $\Omega_0 \geq 1/\sqrt{3}$.

As with the global case, we can determine the initial values of the fields by energy considerations. Neglecting the friction terms, we can write the equations of motion as

$$f'' + \frac{\partial V}{\partial f} = 0, \quad A'' - \frac{\partial V}{\partial A} = 0. \quad (34)$$

This means that the quantity

$$\mathcal{E} = \frac{1}{2} f'^2 - \frac{1}{2} A'^2 + V(f, A) \quad (35)$$

is conserved as a function of ρ ,

$$\frac{d\mathcal{E}}{d\rho} = f' \left(f'' + \frac{\partial V}{\partial f} \right) - A' \left(A'' - \frac{\partial V}{\partial A} \right) = 0. \quad (36)$$

Of course, when the friction is included, this quantity is not conserved and we immediately find that

$$\frac{d\mathcal{E}}{d\rho} = -\frac{2}{\rho} (f'^2 - A'^2). \quad (37)$$

This justifies our interpretation of the term on the right-hand side of the equation as a friction.

For constant f , the potential for A has one extremum at

$$A_{\max} = \frac{\Omega}{\alpha}. \quad (38)$$

Again, Eqs. (24) and (37) indicate that f' and A' affect the energy differently. The f profile behaves according to our usual intuition, but the A kinetic term has the opposite sign. Consequently, as Eq. (38) is a minimum in V , the dynamics of the system drive A uphill either toward $A = 0$ or $A \rightarrow \infty$. If A is larger than A_{\max} , it diverges as $\rho \rightarrow \infty$, which clearly does not satisfy the Q-ball boundary conditions. This implies that for Q-ball solutions $\Omega - \alpha A > 0$, which has two consequences: first, because the right-hand side of A equation of motion

$$A'' + \frac{2}{\rho}A' = -\alpha f^2(\Omega - \alpha A) \quad (39)$$

is always negative, A is monotonically decreasing for Q-ball solutions [14]. Second, as the system evolves, the negative term under the square root in Eq. (31) becomes smaller so the value of f_+ grows. For some solutions, such as the one shown in Fig. 3, the “force” from the A gradient pushes f uphill toward this growing f_+ .

While the gauge field does affect the total Q-ball dynamics, it seems to play a relatively minor role when f transitions from near one to near zero. This observation suggests a relationship between the global Q-ball solutions and gauged Q-ball solutions. To explore this, we need analytic expressions for A and f . Beginning at the thin-wall limit, we approximate f by a step function, $f(\rho) = 1 - \Theta(\rho - R^*)$, and then solve the equation of motion, Eq. (18), for A . By demanding that $A(\rho)$ and its derivative be continuous at $\rho = R^*$, one finds [14]

$$A(\rho) = \frac{\Omega}{\alpha} \begin{cases} 1 - \frac{\sinh(\alpha\rho)}{\cosh(\alpha R^*)\alpha\rho}, & \rho < R^*, \\ \frac{\alpha R^* - \tanh(\alpha R^*)}{\alpha\rho}, & \rho \geq R^*. \end{cases} \quad (40)$$

Remarkably, this result is a good approximation to the exact gauge field solution even beyond the thin-wall regime.

This result indicates that the derivative of αA is small if the Q-ball radius R^* is large,

$$|\alpha A'(R^*)| = \frac{\Omega}{R^*} \left| \frac{\tanh(\alpha R^*) - \alpha R^*}{\alpha R^*} \right| < \frac{\Omega}{R^*}, \quad (41)$$

which implies that αA is essentially constant over the transition. We can then refine our analysis of the scalar profile by solving the f equation of motion around $\rho \sim R^*$ with a constant A ,

$$f'' + \frac{2}{\rho}f' = \frac{1}{\Phi_0^2(m_\phi^2 - \omega_0^2)^2} \frac{dU}{df} - [\Omega - \alpha A(R^*)]^2 f. \quad (42)$$

Equation (42) is exactly the form of the equation for the global Q-ball, Eq. (7), with the global value of Ω_G given by

$$\Omega_G = \Omega - \alpha A(R^*). \quad (43)$$

Since the derivative of αA is small, it does not contribute significantly to the friction over the transition region. This means that the frictional effects over the transition are also nearly identical to the global case. Since the relation between Ω_G and R^* is determined by the friction, if the R^* dependence of the global Q-ball parameter $\Omega_G(R^*)$ is known, we can determine the R^* dependence of the gauged Q-ball $\Omega(R^*)$ via

$$\boxed{\Omega(R^*) = \Omega_G(R^*)\alpha R^* \coth(\alpha R^*)}, \quad (44)$$

where we have used Eq. (43) and the thin-wall formula of Eq. (40) for $A(R^*)$.

Equation (44) is the key result of our paper. It provides a mapping from global Q-balls—for which the relation $\Omega_G(R^*)$ is much easier to obtain both analytically and numerically—and gauged Q-balls with any α . Furthermore, the scalar transition profiles for the gauged Q-balls are expected to be identical to the transition profiles for the corresponding global Q-balls [Eq. (10)]. As we now show, this rather simple argument leads to accurate analytic descriptions of gauged Q-balls.

VI. RESULTS

We can now use these results to construct an analytical estimate for the Q-ball profile. The mapping in Eq. (44) provides the radius of the gauged Q-ball given the known relationship $\Omega_G(R^*)$ from the global Q-ball [Eq. (11) or Fig. 1]. The scalar profile $f(\rho)$ is taken to be the transition profile of global Q-balls [Eq. (10)]; this is well motivated around $\rho \sim R^*$ for large R^* but happens to be a very good approximation for all other cases as well. Finally, the gauge profile $A(\rho)$ is taken from Eq. (40). We can also use this analytical profile to find approximations for Q [via Eq. (20)] and E [via Eq. (24)]; since the resulting expressions are lengthy we do not show them here.

These profiles serve as excellent seed functions for the numerical solution of the differential equations described in Sec. IV. Figure 4 shows a comparison between the numerical calculations and our analytical estimates for one choice of parameters. Note that the two solutions in Fig. 4 have the same potential parameters and scalar frequency ω , but differ in their Q-ball observables such as radius, charge, and energy. These two solutions correspond to the two solutions for R^* obtained from the mapping in Eq. (44). As the plot illustrates, the analytical profiles for f and A match

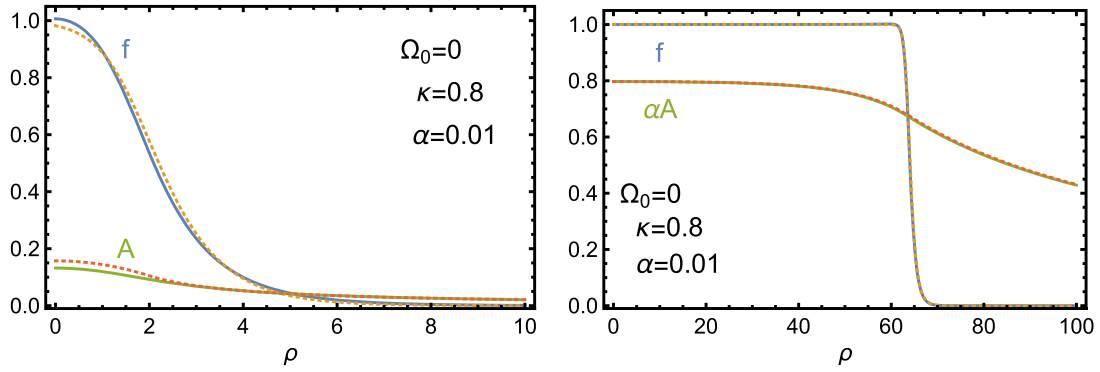


FIG. 4. Profiles for the scalar field and gauge field for a thick-wall (left) Q -ball and a thin-wall (right) Q -ball. The exact numerical results are denoted by the solid lines, while the thin-wall analytic approximation is given by the dashed lines.

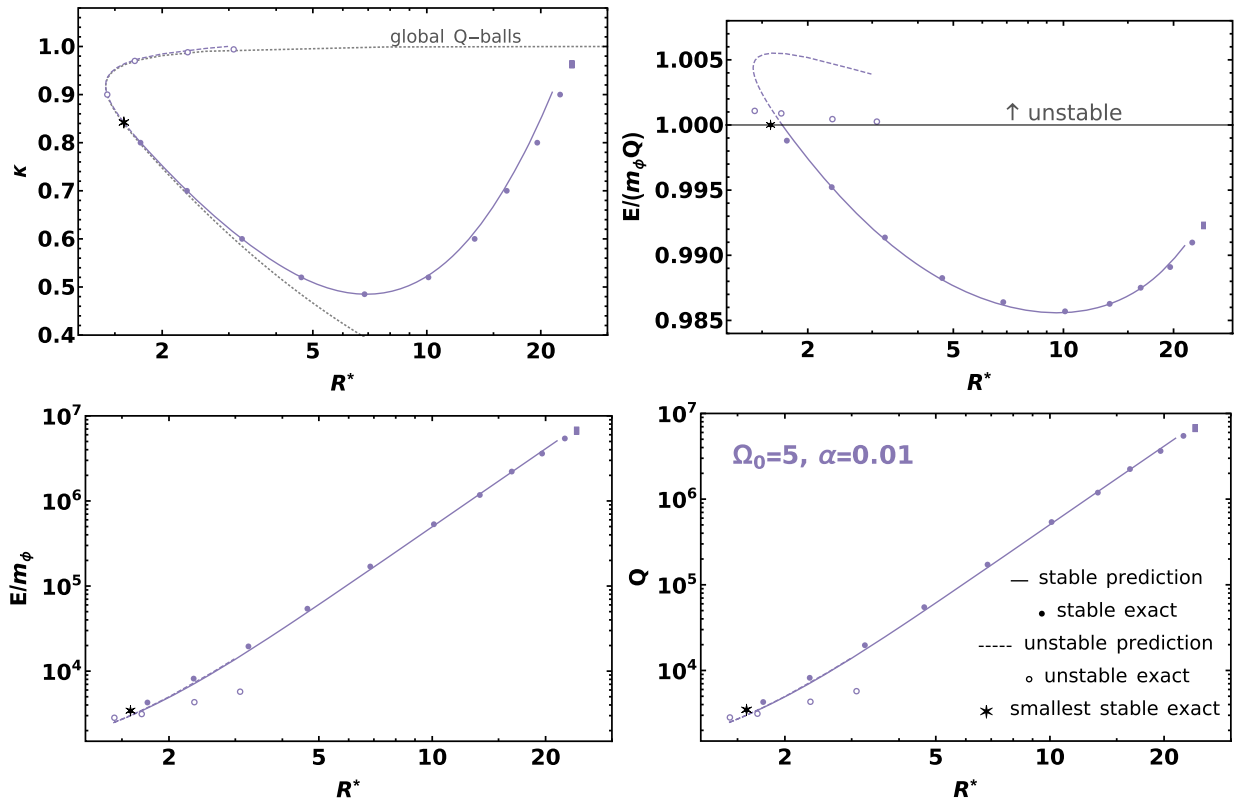


FIG. 5. A comparison of predictions from Eq. (44) and numerical solutions for a sample benchmark $\Omega_0 = 5$, $\alpha = 0.01$, $\phi_0 = m_\phi$. Predicted stable and unstable solutions are shown as solid and dashed lines, respectively, and stable and unstable numerical solutions are shown as filled and open points, respectively. The gray dotted line shows the global Q -ball case. The rectangle shows the largest numerical solution.

the numerical results remarkably well, especially for the large Q -balls (right panel).

We now discuss the Q -ball observables for the benchmark point $\Omega_0 = 5$ and $\alpha = 1/100$; we set $\phi_0 = m_\phi$ throughout and measure all dimensional quantities in units of m_ϕ . The results for this benchmark are shown in Fig. 5. In the top left panel, the numerical results for κ vs R^*

(circles) are compared with the prediction obtained from Eq. (44) (line). The other panels show the analogous results for E/m_ϕ , Q , and $(E/m_\phi Q)$. Overall, there is excellent agreement between the numerical and analytical results.

There are a number of features that restrict the allowable Q -ball solutions. First, we must have $\omega \leq m_\phi$ (or $\kappa \leq 1$) in order for the Q -ball solution to relax to zero for large ρ .

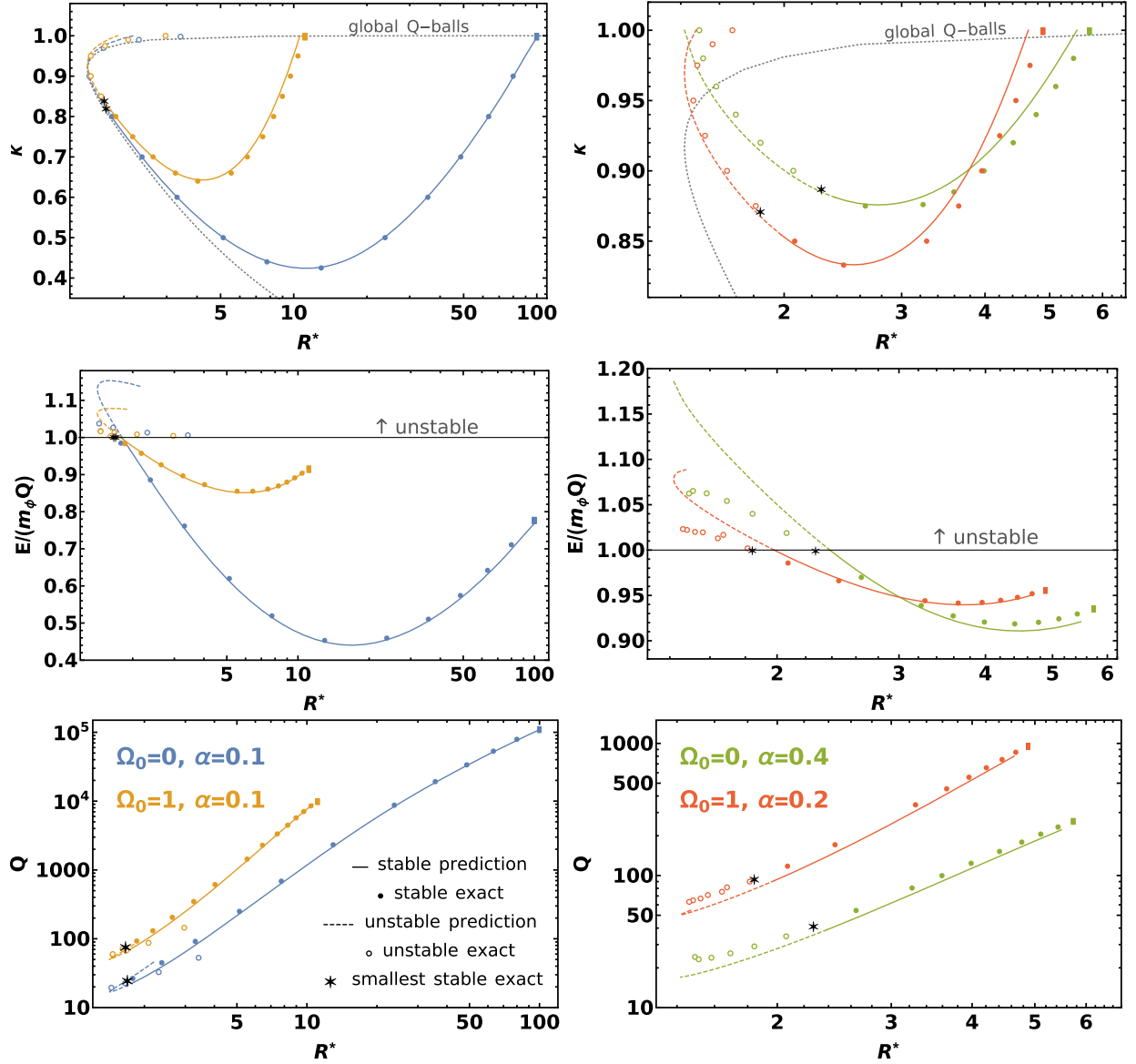


FIG. 6. A comparison of predictions from Eq. (44) and numerical solutions for benchmarks $\Omega_0 = 0, \alpha = 0.1$ (left, blue), $\Omega_0 = 1, \alpha = 0.1$ (left, orange), $\Omega_0 = 0, \alpha = 0.4$ (right, green), and $\Omega_0 = 1, \alpha = 0.2$ (right, red). Conventions are as in Fig. 5.

This typically² implies a maximum Q-ball radius. Second, we must have $E \leq m_\phi Q$ so that the Q-ball is stable against decay to scalars. This constraint is most easily seen in the top right panel of Fig. 5 and implies the existence of a *minimal* Q-ball radius. We have shown this second instability by representing our prediction by a dashed line in the unstable region. The numerical solutions show the same instability; we have represented the last stable solution (the stable solution with smallest R^*) as a star.

²The functional form of $\Omega_G(R^*)$ depends on the scalar potential. Equation (44) implies that $\Omega_G(R^*)$ must fall off faster than $1/R^*$ at large R^* in order to construct gauged Q-balls without a maximal radius. We are not aware of such potentials and global Q-balls in the literature.

Finally, we must impose the constraint of Eq. (33) that demands that the scalar potential have a second maximum away from $f = 0$. This puts an upper bound on the radius which, for this benchmark, is more restrictive than the maximal radius determined by the relation $\omega \leq m_\phi$. Using Eq. (33) with $A = A(0)$ from our thin-wall expression, Eq. (40), we can calculate this maximal radius R_{\max}^* and impose this constraint on our analytical prediction shown in the figure, ending the solid line before $\kappa = 1$. Since the thin-wall $A(0)$ overestimates the true value, our maximal radius is slightly smaller than the true maximal radius (indicated by a rectangle in the plot), but the agreement is still good.

One interesting feature in the κ vs R^* plot is the existence of a minimum allowed value of κ . An analytic expression

for this minimum value can be obtained; since this minimum value must be less than or equal to one for Q-balls to exist, we find the constraint

$$\alpha \lesssim \frac{1}{\sqrt{1/(0.58)^2 + 9\Omega_0^2/2}}. \quad (45)$$

In particular, this predicts that there are no gauged Q-balls with $\alpha > 0.58$. Numerically, we find that the actual upper limit for α is 0.52, in quantitative agreement with the above mapping derivation. Note that it was pointed out in Ref. [14] that for any scalar potential (and its implied attractive force) there must be an upper bound on the allowed gauge coupling (and its implied repulsive force) in order to form a stable Q-ball.

The lower panels of Fig. 5 show the behavior of Q and E as a function of R^* . They inherit both a minimal and a maximal value from the corresponding radius. Our analytical predictions match the numerical results on the (phenomenologically interesting) stable Q-ball branch.

We compare the analytical and numerical data for several other benchmarks in Fig. 6. Our predictions show only small deviations with respect to the numerical results for all benchmarks. This illustrates that the mapping in Eq. (44) holds qualitatively and quantitatively over the whole parameter space.

For these benchmarks, R_{\max}^* is set by the condition $\kappa = 1$ rather than by Eq. (33). Using Eq. (44) and the large- R^* relation $\kappa_G = 1/\sqrt{R^*}$ [13], we find

$$\alpha^2 R_{\max}^* (1 + R_{\max}^* \Omega_0^2) \coth^2(R_{\max}^* \alpha) - \Omega_0^2 = 1. \quad (46)$$

This equation cannot be solved analytically, but has the limiting cases

$$R_{\max}^* \simeq \begin{cases} \frac{1}{\alpha^2}, & \text{for } \Omega_0 \lesssim \alpha, \\ \frac{1}{\alpha \Omega_0}, & \text{for } \Omega_0 \gg \alpha. \end{cases} \quad (47)$$

Since both charge and energy grow with R^* for large radii, this R_{\max}^* also implies a maximal Q-ball charge and energy for a given set of potential parameters. This qualitative claim was made in Ref. [14], but here we provide easy-to-use quantitative predictions.

We also note that in the limiting situation of large R^* , the expressions for charge and energy simplify to

$$Q = \frac{4\pi}{\alpha^2} \Phi_0^2 (\alpha R^* \coth(\alpha R^*) - 1) \sqrt{R^{*2} \Omega_0^2 + R^*}, \quad (48)$$

$$E = \frac{\pi m_\phi R^* \Phi_0^2 \text{csch}^2(\alpha R^*)}{6\alpha \sqrt{\Omega_0^2 + 1}} \times [\alpha R^* (4R^* \Omega_0^2 + 3) - 6(R^* \Omega_0^2 + 1) \sinh(2\alpha R^*) + \alpha R^* (8R^* \Omega_0^2 + 9) \cosh(2\alpha R^*)], \quad (49)$$

as derived in Appendix B. These are more approximate than the full integrals used in our figures, but are significantly more manageable and still make excellent predictions at large R^* .

Using our analytical approximations together with numerical results, we can show that stable gauged Q-balls have $R^* \gtrsim 1.5$, which is similar to the lower limit found for global Q-balls [13]. This matches the physical expectation that the introduction of a repulsive force to a Q-ball should not decrease the Q-ball radius.

We note that for $\Omega_0 = 0$, the scalar profile is found to be essentially constant in the interior of thin-wall Q-balls (Fig. 4, right), and our approximations become more accurate, especially for small α , where the solutions approach the global Q-ball case. For larger Ω_0 , the solutions deviate from the global case (Fig. 2, left), but our results remain accurate. It would be interesting to explore the dependence on Ω_0 further; we leave this to future work.

VII. CONCLUSION

Global Q-balls are curious objects that arise in certain $U(1)$ -symmetric scalar field theories and can be studied analytically and numerically with relative ease. Promoting the $U(1)$ symmetry to a gauge symmetry complicates the discussion significantly and has eluded analytical descriptions outside of some limiting cases.

In this paper, we have exhibited a method to obtain essentially all properties of gauged Q-balls via a mapping from global Q-balls. Since the latter can be easily obtained numerically and often even analytically, this mapping allows for an excellent prediction of the gauged Q-ball properties without the need to solve the coupled, nonlinear differential equations. Our analytical expressions also make possible the solution of the differential equations by finite-element methods rather than the shooting method.

Finally, we stress that our analytical approximations are best in the thin-wall or large-radius limit. Smaller Q-balls show larger deviations, but these are also the Q-balls that are easiest to study numerically, providing good complementarity. Importantly, our analytical approximations also serve as good seed functions for numerical finite-element methods, significantly simplifying the numerical study of thick-wall gauged Q-balls.

ACKNOWLEDGMENTS

This work was supported in part by NSF Grant No. PHY-1915005. C. B. V. also acknowledges support from Simons Investigator Grant #376204. R. R. acknowledges support from the National Science Foundation Graduate Research Fellowship Program under Grant No. 1839285.

APPENDIX A: ENERGY OF GAUGED Q-BALLS

In this appendix, we derive the form of the energy given in Eq. (24). We begin with the Lagrangian and rescale the radial coordinate $\rho \rightarrow \chi\rho$. This yields

$$L = 4\pi\Phi_0^2 \sqrt{m_\phi^2 - \omega_0^2} \int d\rho \rho^2 \chi \left[-\frac{1}{2}f'^2 + \frac{1}{2}A'^2 + \chi^2 V(f, A) \right], \quad (\text{A1})$$

where $V(f, A)$ is defined in Eq. (16). We now consider the variation of the Lagrangian with respect to χ and then set $\chi = 1$. The variation has two parts, first the explicit dependence on χ and second the variation that appears because functions now depend on χ , $f(\rho) \rightarrow f(\rho\chi)$. This second collection of terms, with χ then set to one, is simply the usual variation of the Lagrangian and so vanishes by definition. Requiring the other term in the variation to also vanish yields the constraint

$$0 = \int d\rho \rho^2 \left[-\frac{1}{2}f'^2 + \frac{1}{2}A'^2 + 3V(f, A) \right]. \quad (\text{A2})$$

We can use this constraint to remove the explicit dependence on $U(f)$ from the energy in Eq. (23),

$$\begin{aligned} E &= 4\pi\Phi_0^2 \sqrt{m_\phi^2 - \omega_0^2} \\ &\quad \times \int d\rho \rho^2 \left[\frac{1}{3}f'^2 + \frac{2}{3}A'^2 + f^2(\alpha A - \Omega)^2 \right] \\ &= 4\pi\Phi_0^2 \sqrt{m_\phi^2 - \omega_0^2} \\ &\quad \times \int d\rho \rho^2 \left[\frac{1}{3}f'^2 + \frac{2}{3}A'^2 + \frac{1}{\alpha\rho^2}(\alpha A - \Omega)(\rho^2 A')' \right], \end{aligned} \quad (\text{A3})$$

where in the last line we have used the A equation of motion in (18). The third term is then integrated by parts to produce

$$\frac{E}{\sqrt{m_\phi^2 - \omega_0^2}} = \Omega Q + \frac{4\pi\Phi_0^2}{3} \int d\rho \rho^2 (f'^2 - A'^2). \quad (\text{A4})$$

This result is useful in that it only depends on the change in f and A . Alternatively, the form

$$\frac{E}{\sqrt{m_\phi^2 - \omega_0^2}} = \Omega Q + 8\pi\Phi_0^2 \int d\rho \rho^2 V(f, A) \quad (\text{A5})$$

can also be used to determine the energy without any use of the derivatives of f and A .

APPENDIX B: AN ALTERNATIVE MAPPING DERIVATION

As an alternative to the derivation of the mapping equation (44) in Sec. V we provide here a derivation in the thin-wall limit, i.e., for large R^* . For this, we consider the simplest thin-wall ansatz for the profiles [14], where f is a step function, $f(\rho) \simeq 1 - \Theta(\rho - R^*)$, and A is given by Eq. (40). We can easily integrate these functions to obtain the charge Q [14],

$$Q = \frac{4\pi\Omega\Phi_0^2}{\alpha^3} (\alpha R^* - \tanh(\alpha R^*)), \quad (\text{B1})$$

and the energy [Eq. (24)],

$$\begin{aligned} E &= \omega Q + \frac{\pi\phi_0^2}{3\sqrt{m_\phi^2 - \omega_0^2}} R^{*2} - \frac{4\pi\phi_0^2}{3\sqrt{m_\phi^2 - \omega_0^2}} \\ &\quad \times \frac{\Omega^2(\alpha R^*(\text{sech}^2(\alpha R^*) + 2) - 3\tanh(\alpha R^*))}{2\alpha^3}, \end{aligned} \quad (\text{B2})$$

using the results from Ref. [13] to properly integrate over the discontinuous f'^2 . Notice that the last term in E goes to zero for $\alpha \rightarrow 0$, leading back to the global case. Now we can use Eq. (25) in the form $dE/dR^* = \omega(R^*)dQ/dR^*$ to obtain—and solve—a differential equation for $\omega(R^*)$, yielding

$$\omega(R^*) = \coth(\alpha R^*) \sqrt{cR^{*2} + \alpha^2(m_\phi^2 - \omega_0^2)R^*}. \quad (\text{B3})$$

Here, c is an integration constant that is difficult to obtain, but we can get $c = \alpha^2\omega_0^2 + \mathcal{O}(\alpha^3)$ from matching to the global case $\kappa^2 \simeq 1/R^*$ (valid roughly for $R^* > 2$). This gives us

$$\omega(R^*) = \alpha R^* \coth(\alpha R^*) \sqrt{\omega_0^2 + \frac{m_\phi^2 - \omega_0^2}{R^*}}, \quad (\text{B4})$$

which is identical to the more general mapping formula in Eq. (44) in the large R^* limit due to $\omega_G \simeq \sqrt{\omega_0^2 + \frac{m_\phi^2 - \omega_0^2}{R^*}}$ [13].

- [1] S. R. Coleman and Q. Balls, *Nucl. Phys.* **B262**, 263 (1985); Erratum, *Nucl. Phys.* **B269**, 744 (1986).
- [2] E. Nugaev and A. Shkerin, Review of non-topological solitons in theories with $U(1)$ -symmetry, *J. Exp. Theor. Phys.* **130**, 301 (2020).
- [3] T. D. Lee and Y. Pang, Nontopological solitons, *Phys. Rep.* **221**, 251 (1992).
- [4] A. Kusenko and M. E. Shaposhnikov, Supersymmetric Q balls as dark matter, *Phys. Lett. B* **418**, 46 (1998).
- [5] A. Kusenko and P. J. Steinhardt, Q Ball Candidates for Self-interacting Dark Matter, *Phys. Rev. Lett.* **87**, 141301 (2001).
- [6] E. Pontón, Y. Bai, and B. Jain, Electroweak symmetric dark matter balls, *J. High Energy Phys.* **09** (2019) 011.
- [7] Y. Bai, A. J. Long, and S. Lu, Tests of dark MACHOs: Lensing, accretion, and glow, *J. Cosmol. Astropart. Phys.* **09** (2020) 044.
- [8] G. Rosen, Dilatation covariance and exact solutions in local relativistic field theories, *Phys. Rev.* **183**, 1186 (1969).
- [9] S. Theodorakis, Analytic Q ball solutions in a parabolic-type potential, *Phys. Rev. D* **61**, 047701 (2000).
- [10] R. MacKenzie and M. B. Paranjape, From Q -walls to Q -balls, *J. High Energy Phys.* **08** (2001) 003.
- [11] I. E. Gulamov, E. Ya. Nugaev, and M. N. Smolyakov, Analytic Q -ball solutions and their stability in a piecewise parabolic potential, *Phys. Rev. D* **87**, 085043 (2013).
- [12] A. Masoumi, K. D. Olum, and B. Shlaer, Efficient numerical solution to vacuum decay with many fields, *J. Cosmol. Astropart. Phys.* **01** (2017) 051.
- [13] J. Heeck, A. Rajaraman, R. Riley, and C. B. Verhaaren, Understanding Q -balls beyond the thin-wall limit, *Phys. Rev. D* **103**, 045008 (2021).
- [14] K.-M. Lee, J. A. Stein-Schabes, R. Watkins, and L. M. Widrow, Gauged Q balls, *Phys. Rev. D* **39**, 1665 (1989).
- [15] I. E. Gulamov, E. Ya. Nugaev, A. G. Panin, and M. N. Smolyakov, Some properties of $U(1)$ gauged Q -balls, *Phys. Rev. D* **92**, 045011 (2015).
- [16] Y. Brihaye, A. Cisterna, B. Hartmann, and G. Luchini, From topological to nontopological solitons: Kinks, domain walls, and Q -balls in a scalar field model with a nontrivial vacuum manifold, *Phys. Rev. D* **92**, 124061 (2015).
- [17] I. Gulamov, E. Nugaev, and M. Smolyakov, Theory of $U(1)$ gauged Q -balls revisited, *Phys. Rev. D* **89**, 085006 (2014).
- [18] A. Yu. Loginov and V. V. Gauszstein, Radially excited $U(1)$ gauged Q -balls, *Phys. Rev. D* **102**, 025010 (2020).
- [19] A. G. Panin and M. N. Smolyakov, Problem with classical stability of $U(1)$ gauged Q -balls, *Phys. Rev. D* **95**, 065006 (2017).
- [20] Wolfram Research, Inc., *Mathematica*, Version 12.2, Champaign, IL, 2020, <https://www.wolfram.com/mathematica>.